8-27-2010

Mechanochemistry of Hexagonal Boron Nitride: 1. Destruction and Amorphization During Mechanical Treatment

A. N. Streletskii
Russian Academy of Sciences

D. G. Permenov
Federal State Unitary Enterprise

Kiril A. Streletzky
Cleveland State University, K.STRELETZKY@csuohio.edu

B. B. Bokhonov
Russian Academy of Sciences

A. V. Leonov
Moscow State University

Publisher's Statement

The final publication is available at Springer via http://dx.doi.org/ 10.1134/S1061933X10040162

Mechanochemistry of Hexagonal Boron Nitride: 1. Destruction and Amorphization during Mechanical Treatment

A. N. Streletskii D. G. Permenov K. A. Streletzky , B.B. Bokhonov , and A. V. Leonov

Abstract—The regularities of the mechanical activation of hexagonal boron nitride are analyzed using the X-ray diffraction, IR spectroscopy, transmission electron microscopy, dynamic light scattering, and adsorption methods. At the initial state of mechanical activation, the main process is material destruction. At this stage, the specific surface area increases to 400 m^2/g and crystallographically oriented nanosized needles are formed. At the same time, boron nitride crystal structure is disordered with an increase in interplanar distance $d(002)$. The disordering is assumed to be due to a shift along planes (001). At a specific dose of supplied mechanical energy above 6–8 kJ/g, the disordering processes dominate and the material is amorphized. At this stage, the specific surface area of samples decreases.

INTRODUCTION

There are four crystalline modifications of boron nitride, namely, cubic (c-BN), wurtzite (w-BN), hexagonal (h-BN), and rhombohedral (r-BN). These modifications are absolutely identical to corresponding modifications of carbon, i.e., diamond (cubic form), hexagonal diamond (wurtzite form), and hexagonal and rhombohedral graphite. c-BN and w-BN are hard, dense phases in which boron and nitrogen atoms occur in a tetrahedral coordination, and their chemical bonds are strong and characterized by sp^3-hybridization. h-BN and r-BN, which are noticeably softer, consist of graphite-like layers of planar B_3N_3 hexagons. In h-BN, the ABAB layer sequence is realized, that is, an atom of a complementary type is located over each boron (or nitrogen) atom. In h-BN, the B–N bond length and the distance between hexagon layers are 1.45 and 3.30 Å, respectively. The interlayer bond energy is 4 kcal/mol. Sometimes, h-BN is referred to as white black; it is an insulator and has a melting temperature of 3000°C and a density of 2.3 g/cm^3.

In addition, two disordered forms of boron nitride may be noted; they are turbostrate (t-BN) [1] and amorphous (a-BN) modifications. In the turbostrate form, hexagon layers are located parallel to one another; however, the azimuthal arrangement of the hexagons is chaotic. The crystallographic structure of t-BN is sometimes characterized by two-digit indices (01) and (10), which stress the absence of a three-dimensional symmetry. The disorder in the arrangement of hexagon layers is accompanied by a rise in interlayer distance d_{002}. The t-BN phase, which is characterized by small sizes of the coherent-scattering region (CSR), and the a-BN phase are difficult to distinguish between by the X-ray diffraction methods.

h-BN is promising as a carrier of catalysts [2] and a material for producing nanotubes [3], hydrogen storage [4], and other applications. The interest that has recently arisen in the mechanical activation of h-BN is due to the possibility of facilitating the production of superhard c-BN [5], enhancing the BN sorption capacity with respect to hydrogen [6], decreasing the temperature of nanotube synthesis [7], etc. The production processes and reactivity of Al–BN [8–10], Ti–BN [10–12], Fe–BN [13–14], and Mg–BN [10] layered nanocomposites have been investigated in detail. The formation regularities of nanocomposites in Me–h-BN and Me–C (Me is a metal and C is graphite) have been shown to have a great deal in common [15].

Despite the high interest in the possibilities of using mechanically activated BN and its mixtures, the regularities of the mechanical activation of boron nitride and its reactivity have been poorly studied. The data on the mechanical activation of h-BN were first

obtained in [5, 9, 16–19]. It was shown that the sizes of CSR decreased, the interlayer distance $d(002)$ increased, and various defects arose in the material. A question remains being debatable whether the amorphous state is reached during the mechanical activation of h-BN [5, 19] or the defective structure is confined to a nanocrystalline state [16].

In this series of works, various methods (X-ray diffraction, scanning and transmission electron microscopy, adsorption measurements, dynamic light scattering, IR spectroscopy, differential scanning calorimetry, differential thermogravimetry, elemental and chemical analyses, etc.) are employed to investigate the mechanical activation of h-BN and its reactivity with respect to water, hydrogen, and oxygen. In the first communication, we analyze the regularities of the destruction and amorphization of h-BN upon its activation in an inert atmosphere.

EXPERIMENTAL

h-BN was subjected to mechanochemical activation in mills of three types with different designs and power consumptions. The activation conditions in different mills are presented in the table. The majority of the experiments were performed in a mill of Aronov's design (table, no. 1). In all cases, mechanochemical activation was carried out in an inert atmosphere (Ar, He).

The degree of mechanochemical activation was characterized by specific dose D (kJ/g) of supplied mechanical energy [20]. The dose was calculated using the following relation:

$$D = Jt,$$

where J is the power consumption in a mill and t is the duration of grinding. The J values of the mills were measured by the test-object method [21].

Changes in the crystal structure were registered by the X-ray diffraction method with a DRON-3 instrument using monochromated CuK_α radiation. The values of SCR, L, and microdeformation ε were calculated based on the analysis of the pattern of the X-ray diffraction spectral lines in terms of the Villiams–Hall approximation using the Outset 3 and Profile [22] software packages. For very broad lines, the L values were estimated applying the Scherrer formula. Geometrical broadening was taken into account using well-crystallized aluminum samples.

The specific surface area of boron nitride powders was measured by low-temperature (77 K) Ar adsorption and calculated by the BET method. Transmission electron microscopy (TEM) studies were carried out with a Jeol JEM 2000 FX II microscope. Transmission IR spectra were measured on an AF-1 FT spectrometer. Dynamic light scattering (DLS) was measured using an Ar^+ laser operating at a power of 1 W and a radiation wavelength of 514.5 nm equipped with a BI 200SM multiangle photometer (installed on the goniometer) and a BI-9000 correlator. Suspensions of activated BN powders were prepared in methanol for measurements. The data obtained were analyzed with the help of the CONTIN algorithm, which was used to determine relaxation rate distributions $A(\Gamma)$ from the correlation functions through the inverse Laplace transformation.

Characteristics of the applied mills: V is the cylinder volume; m and M are the masses of a material sample and loaded balls, respectively; and J is the power consumption in the mills

No.	Types of mills	V, cm^3	m, g	M/m	J, W/g
1	Aronov's vibratory	250	5	60 : 1	36
2	planetary-type (Pulverizette-7)	150	5	14 : 1	3.3
3	microvibratory	50	1	27 : 1	0.76

Initial h-BN samples (a purity of 99%) were single-crystal pellets with diameters of 300–500 nm, thicknesses of 70–80 nm, and a specific surface area of 12 m^2/g (for details, see [19]).

RESULTS

Specific Surface Area

Isotherms of argon adsorption on mechanically activated h-BN samples are illustrated in Fig. 1a. The measurements were performed at relative pressures of $P/P_s \le 0.3$ (P_s is the saturation gas pressure at 77 K). Specific surface area S was calculated from these isotherms via the BET equation. The dependence of S on dose D is presented in Fig. 1b. At an initial stage of activation, i.e., at doses below approximately 6 kJ/g, S increases to reach a value of about 400 m^2/g and, after which it decreases.

In addition, isotherms of nitrogen adsorption were measured within the P/P_s range 0.000375–0.875 for a sample with a specific surface area of S = 124 m^2/g, which was determined by the BET method as described above. These data were analyzed in terms of the BET and Dubinin–Radushkevich equations. The analysis performed by the BET method yielded a close value for the specific surface area (125 m^2/g), while the microporosity (~0.07 cm^3/g) and the adsorption activation energy (E = 9.6 kJ/mol) were estimated using the anamorphosis of the Dubinin–Radushkevich equation. Hence, the microporosity is insubstantial and the BET analysis reflects mainly the external surface of the sample, which is accessible to gas.

For different experiments, the data on argon adsorption were normalized relative to the maximum S value (see Fig. 1a). It can be seen that, despite that the specific surface area (and, hence, the adsorption value) changes by almost an order of magnitude, the normalized data lie in the same curve within the measurement error. This finding allows us to believe that, at all doses, the contribution of microporosity to the sorption capacity remains insubstantial.

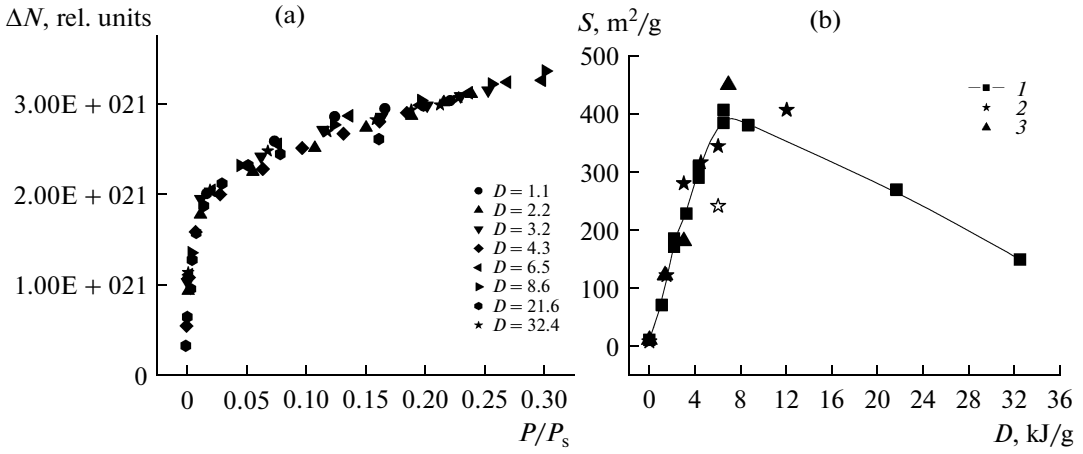

Fig. 1. Panel (a): isotherms of argon adsorption on h-BN samples mechanically activated at different doses D (kJ/g) normalized relative to the maximum value of specific surface area according to BET and panel (b): dependence of S on dose D at a mill power consumption of (*1*) 36, (*2*) 3.3, and (*3*) 0.76 W/g.

The specific surface area of activated h-BN (Fig. 1b) is governed by the dose and is independent of the power consumption and the type of a mill. Despite the power consumptions differ by almost two orders of magnitude (J_1, J_2, and J_3 are 36, 3.3, and 0.76 W/g) and mills of different types (vibratory or planetary-type mill) are applied, all points fall on the same curve.

On the other hand, S may decline during a long storage of an activated sample in air or its contact with air in the course of grinding. For example, in the experiment denoted by asterisks in Fig. 1b, after h-BN was activated at a dose of 4.5 kJ/g, the crushing cylinder was opened, the sample contacted with air, and the mechanical treatment was continued. This operation led to a subsequent reduction in the specific surface area (denoted by an empty asterisk in Fig. 1b). In a control experiment (without the contact of boron nitride with atmosphere), at $D = 6$ kJ/g, S turned out to be higher than that at $D = 4.5$ kJ/g. It appeared that the aforementioned decrease in the specific surface area results from the interaction of atmospheric water vapor with the activated h-BN sample. The water–activated h-BN interaction will be considered in greater detail in the next communication [24].

X-Ray Diffraction

As was mentioned above, the initial h-BN samples represented single-crystal plates (pellets) 300–500 nm in diameter and 70–80 nm thick [19]. Lines 002 and 004 are broadened noticeably stronger than line 100 in the diffractograms of the initial samples. The analysis of the broadening of the 002/004 pair of lines yielded L (CSR) = 84 ± 15 nm ($\varepsilon = 0.1 \pm 0.02$). It can be believed that the planar sides of the pellets correspond to basal plane (001). The spectrum is strongly textured and the intensities of lines 002 and 004 markedly exceed the standard values.

Diffractograms of mechanically activated h-BN are demonstrated in Fig. 2. Diffractograms presented in Figs. 2a and 2b correspond to the stages of an increase and a decrease in the specific surface area in Fig 1b, respectively. The mechanical activation of h-BN is accompanied by the broadening of the lines in the diffractograms, a shift of reflections 002 and 004 toward smaller angles and reflection 100 toward larger angles, and the development of anisotropy in the shape of lines 002 and 100. Boron nitride amorphization dominates in the region of a reduction in the specific surface area, and two wide halos arise in the diffractograms. At the maximum dose $D = 39$ kJ/g, an additional line is registered at 45° due to impurities of iron resulting from the wear of ball and cylinder materials.

For activated h-BN samples, the shape of line 002, which demonstrates anisotropy directed toward smaller angles, cannot be interpreted as one singlet. It appeared that the line shape is most adequately described by introducing three singlets with the area of the main singlet (1) amounting to 70–80% of the total area. The other two singlets are located at smaller angles; the smaller the angle, the broader the singlet. In a subsequent analysis, attention will mainly be focused on the main singlet (1).

Figure 3 presents interlayer distances d(002) observed at different doses as determined from the positions of the most intense singlets (1). At the stage of increasing specific surface area, d(002) rises from 3.343 to 3.375 Å, while, upon h-BN amorphization, the formal value of d(002) becomes as large as 3.6 Å.

The sizes of CSR in the [001] and [100] directions are shown in Fig. 4 as functions of the dose. The CSR sizes were assessed from the half-widths of the main singlets applying the Scherrer formula. In the [001] direction, the CSR sizes diminish to ≈100 Å at the stage of a rise in the specific surface area. In the course of h-BN amorphization, the lines continue to broaden

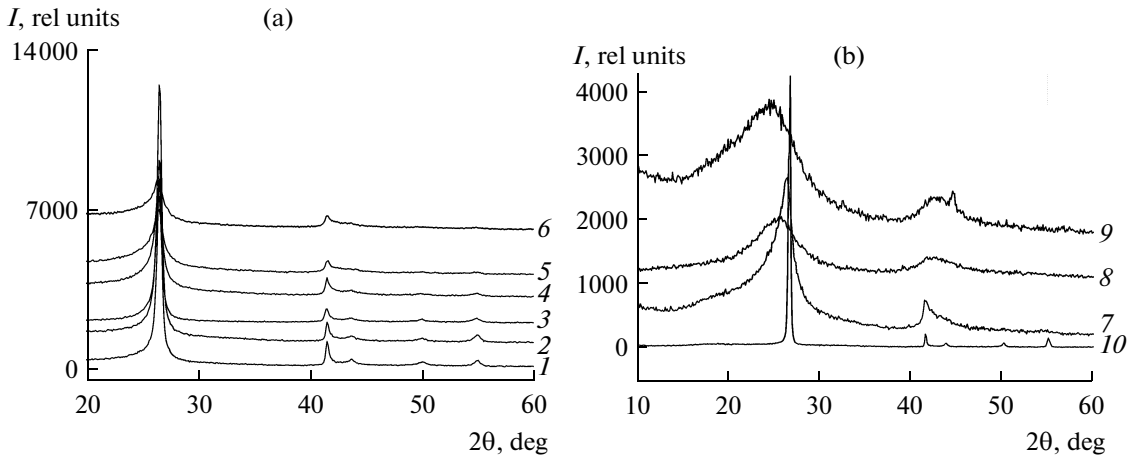

Fig. 2. Diffractograms of mechanically activated h-BN at the stages of (a) destruction and (b) amorphization: Doses: (*1*) 1.4, (*2*) 2.16, (*3*) 3, (*4*) 4.3, (*5*) 6, (*6*) 6.9, (*7*) 8.6, (*8*) 25, (*9*) 32 kJ/g, and (*10*) initial h-BN.

and, at the maximum dose, the formally calculated width of CSR is 12–15 Å. One should note the pronounced anisotropy of CSR sizes. At the stage of growing specific surface area, the CSR sizes in the [100] direction are at least fivefold larger than those in the [001] direction.

It is known [25, 26] that, for rather broad lines registered at small angles of measurements, the line profile is distorted due to the Lorentz, polarization, absorption, and atomic scattering factors, while the line maximum shifts toward smaller angles. In order to correct the profile of line 002, a computer program with the necessary corrections was developed based on formulas (1)–(5) presented in [26]. However, it appeared that allowance for these corrections does not make it possible to describe line 002 of activated BN samples by one singlet and leads to no principle changes in the position of the main singlet. For example, points relevant to experiments 2 and 1 (Fig. 3) correspond to the results of the analyses performed with and without allowance for the correction of the line shape, respectively. It can be seen that the results coincide with each other within the measurement error.

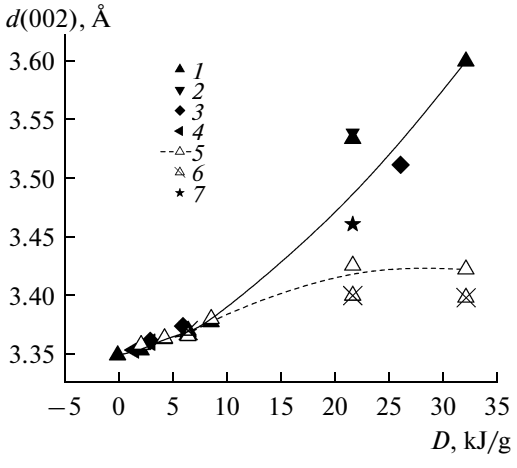

Fig. 3. Interlayer distance *d*(002) of BN as a function of supplied mechanical energy *D*: power consumptions in mills of (*1, 2, 5 7*) 36, (*3*) 0.76, and (*4*) 3.3 W/g; (*7*) post-activation heating under He at 1100°C; and dissolution in (*5*) cold and (*6*) hot water.

IR Spectroscopy

The IR spectra of boron nitride are demonstrated in Fig. 5. Two bands at ~820 and ~1370 cm^{-1} are registered for initial h-BN (spectrum *1*). According to [27], the band with a maximum at 1370 cm^{-1} corresponds to the in-plane vibrations of B_3N_3 hexagons, while the band at 817 cm^{-1} is attributed to the vibrations between the hexagon layers. Mechanical activation causes a shift in the band at 820 cm^{-1} toward lower fre-

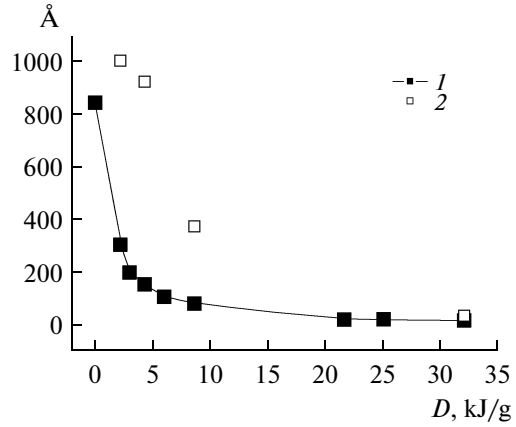

Fig. 4. Sizes of CSR in the (*1*) [001] and (*2*) [100] directions for h-BN activated at different doses of supplied mechanical energy.

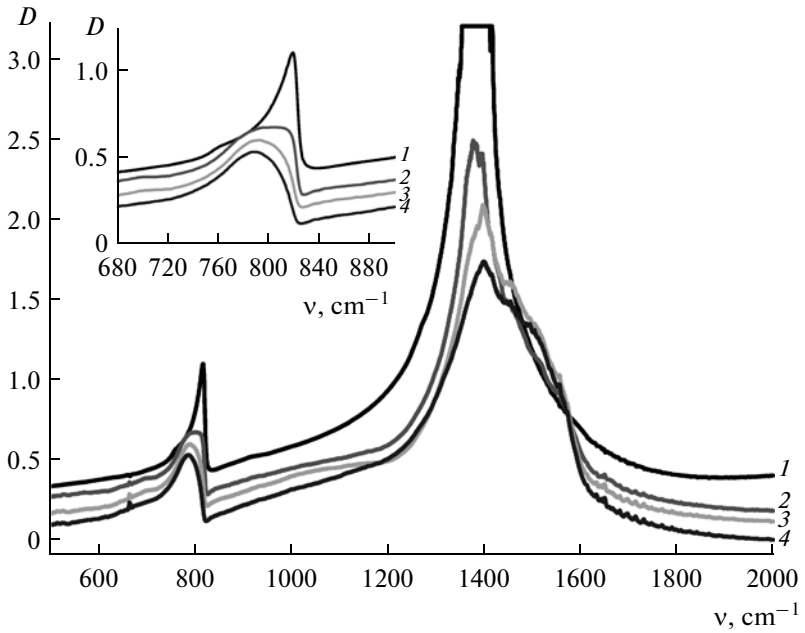

Fig. 5. IR spectra of (*1*) initial h-BN and (*2 4*) h-BN mechanically activated at different doses of supplied mechanical energy: (*2*) 10.8, (*3*) 21.6, and (*4*) 32.4 kJ/g.

quencies and the appearance of several new bands (e.g., at 1500 cm^{-1}, spectra *2–4*). The inset illustrates the spectral range 680–900 cm^{-1} in an expanded scale. At a dose of 10.8 kJ/g (spectrum *2*), the band at 820 cm^{-1} markedly changes its shape. At the maximum dose of 22.3 kJ/g, this band shifts by approximately 30 cm^{-1}. The shift of the band at 820 cm^{-1} toward lower frequencies may be due to an increase in interlayer distance d_{002} and a decrease in the CSR size. It was shown [28] that, due to the enlargement of d_{002} from 3.33 to 3.53 Å, the band shifts by 12 cm^{-1}, while due to the narrowing of CSR by several nanometers, the shift of the band does not exceed 20–25 cm^{-1}. We believe that, in our case, both of these factors contribute to the shift of the band. As was mentioned above, several additional bands arise in the IR spectra of h-BN as a result of mechanochemical treatment. The new bands turned out to be associated with the hydrolysis of activated boron nitride under the action of atmospheric water vapor during its storage in air (for details, see [24]).

Electron Microscopy and Microdiffraction

Initial h-BN samples represented single-crystal pellets. This fact was confirmed by their TEM micrographs and the presence of point reflections in the electron diffraction patters [19, Fig.1].

Figure 6 depicts the TEM micrographs and microdiffractograms obtained for three samples of mechanically activated h-BN. The sample activated at a dose of about 2 kJ/g represents needle-like crystals 5–20 nm thick (Fig. 6a). The electron diffraction pattern of this sample (Fig. 6c) is composed of circular reflections corresponding to polycrystalline BN. For the circular reflections, the calculation of interplanar distances yielded values of 3.33, 2.16, 2.07, and 1.82 Å, which are in good agreement with the data on h-BN. After activation at a dose of 4.3 kJ/g, the needle-like formations (Fig. 6b) became noticeably smaller (the sizes of the majority of the needles are less than 5 nm) and, in addition to the reflections of polycrystalline boron nitride, an amorphous halo arose in the electron diffraction patterns (Fig. 6d). Needle-like formations are very scarce in the TEM micrographs of a sample activated at a dose of 21 kJ/g (Fig. 6e). The typical picture is composed of irregular-shaped aggregates with sizes of grains (primary particles) of 10–30. The electron diffraction patterns of this sample (Fig. 6f) demonstrate only circular reflections of an amorphous type.

Thus the TEM and microdiffraction data suggest that, at the stage of an increase in specific surface area *S*, i.e., at doses lower than 5 kJ/g, activated h-BN samples represent nanosized needle-like polycrystalline formations, while at the stage of decreasing *S*, i.e., at doses above 20 kJ/g, the material is almost completely amorphized. TEM studies always encounter the problem of the extent to which an observed local structure is typical of the entire activated material. Therefore, the TEM data were supplemented with the measurement of DLS, which enabled us to judge the characteristic sizes of the majority of particles.

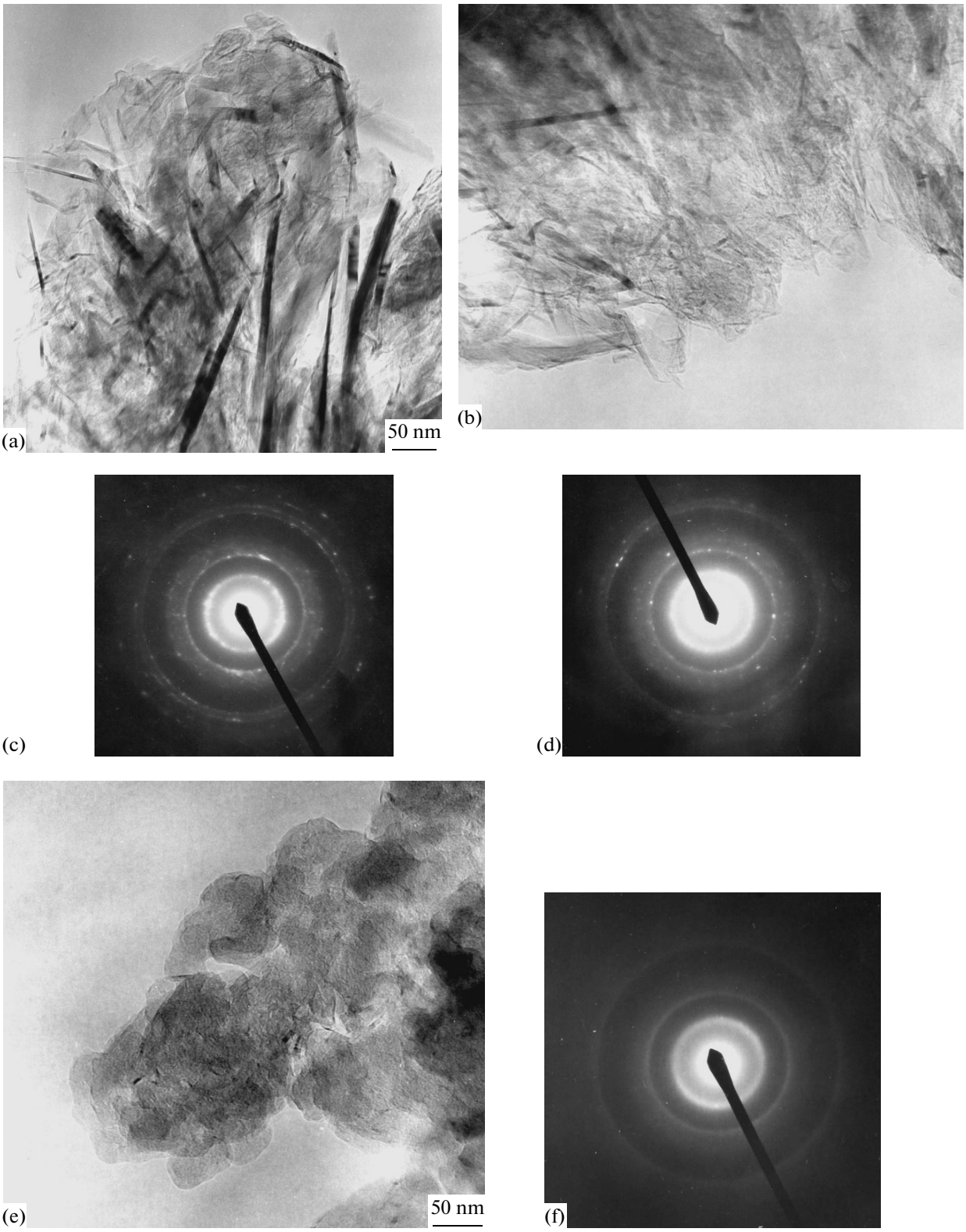

Fig. 6. (a, b, e) TEM micrographs and (c, d, f) microdiffraction patterns for h-BN mechanically activated at different doses of supplied energy: (a, c) 2, (b, d) 4.3, and (e, f) 21.6 kJ/g.

Dynamic Light Scattering

DLS is a nondestructive method for studying the structure and dynamics of complex liquids, suspensions, liquid crystals, and the processes of nanocrystal nucleation and growth. In the DLS, the scattered light intensity is measured as a function of time, and the fluctuations of particle concentration in a solution are registered under the conditions of thermodynamic equilibrium [23]. Correlation functions are calculated and analyzed based on the fluctuation intensities. Translational D_{tr} and rotational Ξ diffusion coefficients of particles in a liquid are determined from the decay rate of correlation function Γ, and the distributions of effective hydrodynamic radii (or effective hydrodynamic sizes for extended objects) are calculated from the diffusion coefficients. Prior to measurements, an h-BN sample activated at a dose of 4.3 kJ/g was dispersed in methanol. During the measurements, the temperature in the measuring cell was 24.4°C. In order to verify the assumption that particles were anisotropic, DLS was measured at different scattering angles in the range 40–130°.

Normalized correlation functions are demonstrated in Fig. 7a for scattering angles of 40, 60, 90, 120, and 130°. The nonexponential pattern of the correlation function (which is expected for greatly anisotropic particles) was especially pronounced at large angles. Very slow processes observed when analyzing some correlation functions were attributed to impurities and subsequently ignored.

The CONTIN algorithm is the standard method for analyzing nonexponential correlation functions [29]. Using this algorithm distributions of relaxation rates $A(\Gamma)$ were obtained from the correlation functions for different scattering angles through the inverse Laplace transformation. The final distributions of effective hydrodynamic radii R_{eff} are illustrated in Fig. 7b. It is known [29, 30] that anisotropic rodlike particles are characterized by two peaks at large scattering angles, one of which retains its position at all angles, while the other one shifts toward larger R_{eff} values with an increase in the scattering angle. Indeed, the size distributions (Fig. 7b) exhibit only one peak at small angles (40 and 60°C) and two peaks at angles of 90° and above. One of the latter two peaks, which, on average, retains its position ($R_{eff} \sim 100$ nm), demonstrates a diffusion-like dependence of the decay rate Γ ($\Gamma \sim q^2$) at all scattering angles. Hence, it really corresponds to the translational particle diffusion. Another peak, which is located at 600–900 nm, only arises at large scattering angles, shifts toward larger R values, and increases with an increase in the scattering angle. This finding leads us to assume that the system contains nonspherical particles whose rotational diffusion substantially contributes to the latter peak.

The translational diffusion coefficient D_{tr} may be determined from the position of the maximum of the translational peak R_h. The averaging of the data obtained at different angles yielded $D_{tr} = 3.6 \times 10^{-12}$ m^2/s.

Based on the position of the maximum of the second mode of size distribution (to which both rotational and translational motions contribute), we can determine (with due regard to R_h) rotational diffusion coefficients Ξ at different scattering angles [30]. It appeared that $\Xi = 287.8$, 409.4, and 422.7 s^{-1} at 90, 120, and 130°, respectively.

On the other hand, the diffusion coefficients of rods in diluted solutions are described by the following relations derived for translational diffusion [29, 30]:

$$D_{tr} \quad k\frac{T}{6\pi\eta a}G, \qquad (1)$$

where

$$G \quad \ln(2\rho) \quad 0.5$$
$$\times\left[1.46 \quad 7.4\left(\frac{1}{\ln(2\rho)} \quad 0.34\right)^2 \quad 4.2\left(\frac{1}{\ln(2\rho)} \quad 0.39\right)^2\right],$$

and rotational diffusion

$$\theta \quad 3\frac{kT}{16\pi\eta a^3}F, \qquad (2)$$

where

$$F \quad 2\left[\ln(2\rho) \quad 1.45 + 7.5\left(\frac{1}{\ln(2\rho)} \quad 0.27\right)^2\right].$$

Here, $\rho = L/d$ and $a = L/2$, where L and d are the length and diameter of the rod, respectively.

For semidilute solutions of rods, the effective D_{tr} is about 1/2 of the value obtained from Eq. (1) under the assumption of an infinitely diluted solution. Analogously, for semidilute solutions, the Ξ value must be smaller than that calculated through Eq. (2).

Estimations performed using relations (1) and (2) with regard to all of the aforementioned suggested that the measured diffusion coefficients may correspond to needles with thicknesses and lengths of 5.5–10 and 330–380 nm, respectively.

Thus, the DLS measurements confirmed that h-BN activated at a dose of $D = 4.3$ kJ/g mostly consists of rods or needles with thicknesses and lengths of 5.5–10 and 330–380 nm, respectively.

DISCUSSION

At an initial stage of the mechanical treatment of hexagonal boron nitride, the main process is the cleavage of its plates, which is accompanied by an increase in its specific surface area to approximately 400 m^2/g (Fig. 1). According to the adsorption measurements performed in a wide pressure range, the porosity of the samples thus obtained is low, and their specific surface area is, mainly, determined by the external surface of formed particles.

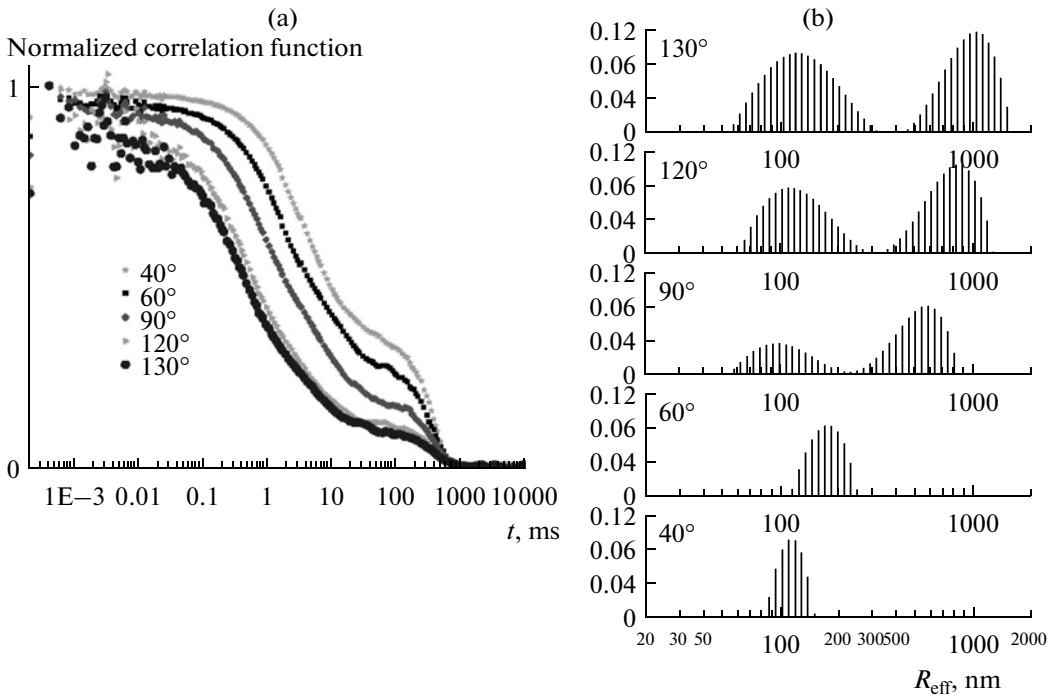

Fig. 7. (a) Correlation functions and (b) particle distributions over hydrodynamic radii measured at different scattering angles for an h-BN sample mechanically activated at $D = 4.3$ kJ/g.

The TEM measurements unexpectedly showed that, at the stage of increasing specific surface area, activated h-BN samples consist of extended needle-like formations whose transverse sizes gradually decrease. According to the TEM data, in an h-BN sample activated at a dose of 4.3 kJ/g, the transverse size of the particles is about 5 nm and their lengths are as much as several hundred nanometers. The DLS measurements (Fig. 7) confirmed that needle-like formations are indeed the main structural elements of the entire activated material and the translational and rotational diffusion coefficients measured for them correspond to an average needle thickness and length of 5.5–10 and 330–380 nm, respectively.

Specific surface area S of long needles with round or square cross sections can be assessed using the following relation: $S \sim 4/\rho h$, where h is the thickness or diameter of a needle. An h-BN sample activated at a dose of 4.3 kJ/g has $S = 310$ m^2/g. In this case, the average thickness of needles is 5.6 nm. In other words, the measured specific area can mainly be related to the external surface of the formed needles.

These needles appeared to have a crystallographic orientation. This conclusion follows from the anisotropic broadening of X-ray diffraction lines. The data presented in Fig. 2 show that line 002 is broadened noticeably stronger than line 100, and the sizes of CSR in the [001] direction are several times smaller than those in the [100] direction (Fig. 4). Therefore, it may be believed that the major axis of formed needles is oriented in the [100] direction. Further studies are necessary to determine the mechanism of the formation astonishing processes of crystallographically oriented needles in the course of mechanochemical activation.

The second process is the disordering of the crystal structure of h-BN. This process primarily leads to an increase in interlayer distance d_{002}, which is determined by the X-ray diffraction analysis (Fig. 3) (based on the position of line 002) and FTIR spectroscopy (Fig. 5) as the shift of the absorption band at 820 cm^{-1} toward lower frequencies. The analysis of the shape of the broadened diffraction lines indicated that particles of the activated sample are characterized by a wide distribution over the degree of imperfection; i.e., in addition to the main fraction, there is a small amount of the material in which the swelling is markedly larger, while the sizes of CSR are smaller. Moreover, the particle distribution over the degree of imperfection affects the character of the IR spectra (see Fig. 5, spectrum *2*). At the stage of an increase in the specific surface area (Fig. 1), the majority of the material remains polycrystalline, which is evident from the pattern of the X-ray spectrum (Fig. 2a) and the microdiffraction data (Fig. 6b). As the dose of supplied mechanical energy is enhanced, the contribution of the turbostrate or/and amorphous fractions increases (Fig. 6d); however, below doses of $D = 6$–8 kJ/g, which correspond to the maximum specific surface area, the d_{002} value is increased only to ~3.38 Å.

At doses above 8 kJ/g, two wide halos (01) and (10) remain preserved in the diffractograms and the widths of the halos continue to increase with D. Halo (01),

which originates from line 002, shifts toward smaller angles. The formally calculated d_{002} value is as large as 3.50–3.52 and 3.6 Å at doses of 20–25 and 32 kJ/g, respectively. Halo (10), which originates from line 100, shifts toward larger angles. It can be believed that, at these doses, boron nitride occurs partly in a turbostrate and partly in an amorphous state. These two fractions can be quantitatively distinguished between with the help of high-resolution transmission electron microscopy.

In may be assumed that boron nitride lattice swells due to a shift along plane (001), which leads to the loss of the mutual orientation of the planes and the transition of h-BN initially to the turbostrate and then to the amorphous phase.

Thus, two stages can be distinguished during the mechanical activation of h-BN. At the initial state, below doses of approximately 6–8 kJ/g, the main process is the cleavage of boron nitride particles and the formation of oriented nanosized needles. At this stage, the specific surface area enlarges to 400 m^2/g. Simultaneously, a shift along plane (001) takes place, which is accompanied by the swelling of the crystal lattice and the gradual amorphization of the material. At doses above 8 kJ/g, the shift process dominates, which leads to the formation of an amorphous nanosized material.

ACKNOWLEDGMENTS

We are grateful to I.V. Povstugar and O.S. Morozova for a number of performed experiments. This work was supported by the Presidium of the Russian Academy of Sciences (program no. 18) and the Russian Foundation for Basic Research (project no. 07-03-00610a).

REFERENCES

1. Tomas, J., Weston, N.E., and O'Connor, T.E., *J. Am. Chem. Soc.*, 1963, vol. 84, p. 4619.
2. Postole, G., Caldararu, M., Ionescu, N.I., et al., *Thermochim. Acta*, 2005, vol. 434, p. 150.
3. Ma, R., Bando, Y., Sato, T., and Kurashina, K., *Chem. Mater.*, 2001, vol. 13, p. 2965.
4. Chen, X., Gao, X.P., Zhang, H., et al., *J. Phys. Chem.,* 2005, vol. 109, p. 11525.
5. Huang, J.Y., Yasuda, H., and Mori, H., *J. Am. Ceram. Soc.*, 2000, vol. 83, p. 403.
6. Lim, S.H., Luo, J., Ji, W., and Lin, J., *Catal. Today*, 2007, vol. 120, p. 346.
7. Ji, F., Cao, C., Xu, H., and Yang, Z., *Chin. J. Chem. Eng.*, 2006, vol. 14, p. 389.
8. Xia, Z.P., Li, Z.Q., Li, C.J., et al., *J. Alloys Compd.*, 2005, vol. 399, p. 139.
9. Streletskii, A.N., Permenov, D.G., Povstugar, I.V., et al., *Khim. Interesah Ustoich. Razvit.*, 2007, vol. 15, p. 175.
10. Povstugar, I.V., Streletskii, A.N., Permenov, D.G., et al., *J. Alloys Compd.*, 2009, vol. 483, p. 298.
11. Ding, Z.H., Yao, B., Qiu, L.X., et al., *J. Alloys Compd.*, 2005, vol. 391, p. 77.
12. Borchers, Ch., Morozova, O.S., Khomenko, T.I., et al., *Chem. Phys. Lett.*, 2008, vol. 465, p. 82.
13. Bokhonov, B., Korchagin, M., and Borisova, Yu., *J. Alloys Compd.*, 2004, vol. 372, p. 141.
14. Tao, J.G., Yao, B., Yang, J.H., et al., *J. Alloys Compd.*, 2004, vol. 384, p. 268.
15. Streletskii, A.N, Kolbanev, I.V., Borunova, A.B., and Butyagin, P.Yu., in *Modern Mechanochemistry, Research Signpost* (in press).
16. Xia, Z.P. and Li, Z.Q., *J. Alloys Compd.*, 2006, vol. 436, p. 170.
17. Taniguchi, T., Kimoto, K., Tansho, M., et al., *Chem. Mater.*, 2003, vol. 15, p. 2744.
18. Du, X.J., Guo, F.Q., and Lu, K., *Nanostruct. Mater.*, 1996, vol. 5, p. 579.
19. Streletskii, A.N., Permenov, D.G., Bokhonov, B.B., et al., *J. Alloys Compd.*, 2009, vol. 483, p. 313.
20. Butyagin, P.Yu. and Pavlichev, I.K., *React. Solids*, 1986, vol. 1, p. 361.
21. Streletskii, A.N., Abstracts of Papers, *2 Int. Conf. on Structural Applications of Mechanical Alloying*, Vancouver, 1993, p. 51.
22. Shelekhov, E.V., Abstracts of Papers, *Nats. konf. po primeneniyu rentgenovskogo i sinkhrotronnogo izlucheniі, neitronov i elektronov dlya issledovaniya materialov* (Natl. Conf. on Application of X-Ray and Synchrotron Radiation, Neutrons and Electrons for Materials Research), Dubna, 1997, vol. 3, p. 316.
23. Berne, B.J. and Pecora, R., *Dynamic Light Scattering*, New York: Wiley, 1976.
24. Streletskii, A.N., Permenov, D.G., Bokhonov, B.B., et al., *Kolloidn. Zh.* (in press).
25. Ziyatdinov, A.V., *Ross. Khim. Zh.*, 2004, vol. 48, no. 5, p. 5.
26. Iwashita, N., Park, C., Fujimoto, H., et al., *Carbon*, 2004, vol. 42, p. 701.
27. Nemanich, R.J., Solin, S.A., and Martin, R.M., *Phys. Rev. B: Condens. Matter*, 1981, vol. 23, p. 6348.
28. Rozenberg, A.S., Sinenko, Yu.A., and Chukanov, N.V., *J. Mater. Sci.*, 1993, vol. 28, p. 567.
29. Zero, K.M. and Recora, R., *Macromolecules*, 1982, vol. 15, p. 87.
30. Flamberg, A. and Pecora, R., *J. Phys. Chem.*, 1984, vol. 88, p. 3026.